Engineering Structures 195 (2019) 96–112

Contents lists available at ScienceDirect

Engineering Structures

journal homepage: www.elsevier.com/locate/engstruct

Out-of-plane seismic safety assessment of URM infills accounting for the in-plane/out-of-plane interaction in a nonlinear static framework

Paolo Ricci, Mariano Di Domenico*, Gerardo M. Verderame

Department of Structures for Engineering and Architecture, University of Naples Federico II, Via Claudio 21, 80125 Naples, Italy

ARTICLE INFO

Keywords:
URM infill wall
Out-of-plane
In-plane/out-of-plane interaction
Nonlinear static analysis
Out-of-plane safety check

ABSTRACT

Past and recent earthquakes showed the occurrence of Out-Of-Plane (OOP) failures of Unreinforced Masonry (URM) infills in Reinforced Concrete (RC) frames. Such a type of failure, which is promoted by In-Plane (IP) damage (IP/OOP interaction), is dangerous for human life safety and its effects can be associated with the attainment of the Life Safety limit state.

In this work, the seismic capacity of Reinforced Concrete buildings at the first OOP collapse is evaluated with a linear analysis based on code provisions and with a procedure based on nonlinear static analysis.

More specifically, 16 buildings designed to Eurocodes, different for number of storeys and design Peak Ground Acceleration (PGA), are infilled by two infill layouts different for thickness and masonry properties. For these buildings, the PGA at which the first OOP infill collapse occurs is evaluated by applying two different approaches. The first is based on linear analysis and consists in the simple application of the demand and capacity models currently provided by the Eurocodes. So, it accounts neither for the effect of the IP/OOP interaction on the OOP capacity nor for the effect of structural non-linearity on the OOP force demand. The second approach is based on nonlinear static analysis and on the application of refined literature formulations accounting for the IP/OOP interaction and for structural non-linearity for the definition of the OOP capacity and force demand.

The PGAs at the OOP collapse of infills obtained by applying both approaches are compared to show their significant overestimation if the IP/OOP interaction and structural non-linearity are not considered, i.e., if current code provisions are applied. Considerations concerning the influence of the number of storeys and of the design PGA of buildings on the PGA at the OOP collapse of infills are reported. Frequency distributions of OOP collapses at different storeys and fragility curves relating the probability of OOP collapse to both the PGA acting in the OOP direction and the maximum IDR attained in the IP direction are shown.

For all case-study buildings, a range of 42 infill layouts, different for thickness and masonry compressive strength, is considered and, with the application of the more refined, not code-based approach, a “limit state” curve defining the infill height-to-thickness ratio/masonry compressive strength couples for which the OOP safety check of infills can be neglected is reported.

1. Introduction

In the Mediterranean area, Reinforced Concrete (RC) buildings are usually provided with Unreinforced Masonry (URM) infill walls. In case of earthquake, these non-structural elements are sensitive to displacement in the In-Plane (IP) direction and to acceleration in the Out-Of-Plane (OOP) direction [1]. IP displacements can damage infill walls and produce the attainment of the Damage Limitation limit state (DL), with significant effects in terms of repairing costs for RC buildings. However, it is common opinion in the engineering community (e.g., [2,3]) that the IP failure of infills, which occurs with crushing and spalling of masonry units, can be also associated with the attainment of Life Safety limit state (LS). The OOP acceleration can produce infills' collapse with their overturning, which is a great risk for life safety and an obstacle to escape/rescue operations during seismic emergency [4]. For this reason, also the OOP collapse of infill walls can be associated with the attainment of LS.

Especially in recent years, analytical and experimental works concerning infills' OOP behaviour, (e.g., among others, [5–16]), have been presented. Based also on these works, some provisions were introduced in the most recent building codes to provide recommendations on infills' verification with respect to OOP seismic actions. Provisions about

* Corresponding author.
E-mail addresses: paolo.ricci@unina.it (P. Ricci), mariano.didomenico@unina.it (M. Di Domenico), verderam@unina.it (G.M. Verderame).

https://doi.org/10.1016/j.engstruct.2019.05.088
Received 5 September 2018; Received in revised form 2 May 2019; Accepted 28 May 2019

Nomenclature

Abbreviations

DA	Designer Approach
DL	Damage Limitation limit state
IDR	Interstorey Drift Ratio
IP	In-Plane
LS	Life Safety limit state
OOP	Out-Of-Plane
PGA	Peak Ground Acceleration
PSA	Pseudo-Spectral Acceleration
RA	Reference Approach
RSA	Response Spectrum Analysis
SDA	Suggested Designer Approach
SL	Strong Layout
WL	Weak Layout

Symbols

a_g	PGA on stiff horizontal soil
d_{crack}	IP displacement at the infill first cracking
d_{max}	IP displacement at the infill peak load
d_u	IP displacement at the infill complete loss of load-bearing capacity
E	elastic modulus
F_{crack}	IP force at the infill first cracking
f_d	design masonry compressive strength
f_m	masonry compressive strength
$f_{m,min}$	minimum masonry compressive strength of OOP safe infills at fixed h/t
F_{max}	IP force at the infill peak load
F_{Rd}	infill OOP strength
G	shear modulus
g	gravity acceleration
H	building total height
h	infill height
h/t	infill slenderness ratio
IDR_{crack}	IDR at the infill IP first cracking
IDR_{max}	IDR at the infill IP peak load
IDR_u	IDR at the infill IP complete loss of load-bearing capacity (IP collapse)
K_{crack}	infill IP initial stiffness
K_{max}	infill IP secant stiffness at peak load
l_a	infill dimension in the direction of arching thrust
PGA_c	PGA at the first OOP infill collapse
$PGA_{c,OOP}$	PGA at the first OOP infill collapse
$PGA_{c,IP}$	PGA at the first IP infill collapse
PGA_{IP}	PGA demand in the IP direction
PGA_{OOP}	PGA demand in the OOP direction
PSA_c	PSA acting on the first infill collapsed due to OOP failure
p	infills' IP softening stiffness normalized with respect to the elastic stiffness
q	behaviour factor for structural design
q_a	behaviour factor associated with the OOP response of infills
R	OOP strength reduction factor
S	soil factor
S_a	pseudo-spectral acceleration in g units
t	infill thickness
T_a	first OOP vibration period of the infill
T_1	first structural vibration period in the OOP direction
V_b	base shear
w	infill width
W_a	infill weight participating to the infill first OOP vibration mode
z	height of the infill barycenter above the building base
α	seismic coefficient (a_g/g)
α_u/α_1	overstrength ratio
γ_a	importance factor of the infill wall
Δ_{TOP}	top displacement of the building
$\Delta_{TOP,RSA}$	top displacement of the building calculated by using RSA at $PGA_{c,OOP}$
$\Delta_{TOP,RA}$	top displacement of the building calculated by using RA at $PGA_{c,OOP}$

or extendable to infills' OOP capacity are reported in Eurocode 6 (EC6) [17], FEMA306 [18] and FEMA 356 [19], ASCE-SEI 41/13 [20] and ASCE-SEI 41/17 [21] while indications concerning the OOP acceleration demand acting on non-structural elements – such as infill walls – based on simplified floor spectra, are provided, for example, in FEMA 356 [19] and Eurocode 8 (EC8) [22]. However, EC6 strength formulation does not account for the IP/OOP interaction phenomena, i.e., the effects of damage due to IP actions on the OOP behavior of infills and vice versa. In fact, many authors showed with analytical and experimental studies how the IP displacement demand affects the OOP response of infills in terms of capacity and demand acting on them [6,23–30].

In this work, 16 RC case-study infilled buildings different for number of storeys (2, 4, 6 and 8) and for the design Peak Ground Acceleration at LS (0.05, 0.15, 0.25 and 0.35 g) are examined. Moreover, two different infill layouts are considered, i.e., a two-leaf (thickness: 80 + 120 mm) 'weak' infill layout and a one-leaf (thickness: 300 mm) 'strong' infill layout. First, for each case-study building, the Peak Ground Acceleration (PGA) at which the first OOP collapse of infills occurs (PGA_c) is assessed according to a "Designer Approach" (DA, i.e., a "code-based" approach) applied in a linear elastic framework on bare frame models and using code provision for the assessment of infills' OOP capacity and demand. Second, the PGA_c is evaluated by using nonlinear static analyses on infilled models of the case-study buildings and literature formulations for the assessment of the OOP capacity and demand by accounting for the IP/OOP interaction, according to the procedure assumed as "Reference Approach" (RA). The influence of the number of storeys and of the design PGA of the building on the PGA_c is discussed. The overestimation of PGA_c if the "Designer Approach" is applied is shown and discussed, as well as the overestimation of PGA_c if it is assessed in a linear elastic framework even if the IP/OOP interaction is considered. Based on the "Reference Approach" results, fragility curves with respect to the first OOP collapse are calculated by considering both the OOP PGA and the IP inter-storey drift ratio (IDR) at collapse as demand parameter. Finally, for all case-study buildings, a wide range of 42 infill layouts, different for slenderness (i.e., height-to-thickness) ratio and masonry compressive strength, is considered and the results of the application of the "Reference Approach" are shown in order to calculate a "limit state" curve defining the slenderness ratio/masonry compressive strength couples for which the OOP safety check of infills may be neglected.

2. Description of the procedures applied for the PGA_C assessment

As previously stated, the first aim of this work is assessing the overestimation of the PGA and of the spectral pseudo-acceleration PSA associated with the first OOP infill collapse (PGA_c and PSA_c, respectively) calculated by neglecting the IP/OOP interaction and by using a totally Eurocode-based approach for 16 RC case-study infilled buildings different for number of storeys (2, 4, 6 and 8) and for the design PGA at

LS (0.05, 0.15, 0.25 and 0.35 g). To achieve this goal, the hereafter-described procedures are applied. In the following, the X and Z global axes define the horizontal reference plan. Consider X as the 'IP direction' and Z as the 'OOP direction'; clearly, the following procedures are applied also considering X as the 'OOP direction' and Z as the 'IP direction'.

Note that the PGA_c is assumed as capacity PGA of the entire building at LS. In other words, the OOP collapse of infills is considered equivalent to the attainment of LS. This is in accordance with section 2.2.2(6)P of EC8, in which it is stated that at Ultimate limit states, such as LS, "*it shall be verified that under the design seismic action the behaviour of non-structural elements does not present risks to persons and does not have a detrimental effect on the response of the structural elements*".

2.1. Designer (code-based) Approach (DA)

For the application of the DA, the OOP strength of infills, F_{Rd}, is calculated by applying EC6 formulation for masonry walls under uniformly-distributed lateral load reported in section 6.3.2, herein extended to infill walls (Eq. (1)).

$$F_{Rd} = f_d \left(\frac{t}{l_a}\right)^2 wh \tag{1}$$

In Eq. (1), t is the infill thickness, w is the infill width, h is the infill height. Infill walls with w > h, as in our case, mainly arch in the vertical direction [8]. For this reason, in Eq. (1) f_d is the design compressive strength of masonry in the vertical direction and l_a is the height of the infill calculated as distance between the confining beams' centerlines.

For each case-study bare frame, the OOP force demand, F_{Ed}, acting on the infills at each storey is assessed by applying Eq. (2), which is proposed in section 4.3.5 of EC8.

$$F_{Ed} = \frac{S_a W_a \gamma_a}{q_a} \tag{2}$$

In Eq. (2), W_a is the weight of the infill participating to its first out-of-plane vibration mode, γ_a is the importance factor of the infill, assumed equal to 1 according to section 4.3.5.3 of EC8, q_a is the behaviour factor of the infill, assumed equal to 2, as suggested for exterior walls in section 4.3.5.4 of EC8. S_a is the seismic coefficient, which is equal to the PSA acting on the infill in the OOP direction divided by gravity acceleration, g. It is calculated as shown in Eq. (3).

$$S_a = \alpha S \left[\frac{3(1 + z/H)}{1 + (1 - T_a/T_1)^2} - 0.5\right] \tag{3}$$

In Eq. (3), α is the design acceleration on type A soil, a_g, divided by gravity acceleration g, S is the soil factor, z is the height of the infill barycenter above the building base, H is the total height of the building, T_1 is the fundamental vibration period of the building in the relevant direction, i.e., in our case, the design fundamental vibration period of the building in the OOP direction, calculated for the bare frame model with halved-inertia for the structural elements' section. T_a is the infill vibration period in the OOP direction. Codes do not provide indications for the calculation of T_a, hence there is no code prescription that can be assumed as reference. For this reason, T_a is calculated, both when applying the DA and the RA, by using the classical formulation for a single-degree of freedom system, with mass equal to the infill mass participating to the first OOP vibration mode (assumed as the 66% of the infill total mass), and stiffness calculated as for an elastic plate pinned along all edges according to the formulation by Timoshenko and Woinowsky-Krieger [31]. With some manipulation, Eqs. (2) and (3) can be written as Eqs. (4) and (5), respectively.

$$F_{Ed} = \frac{PSA}{g}\frac{W_a \gamma_a}{q_a} \tag{4}$$

$$PSA = PGA\left[\frac{3(1 + z/H)}{1 + (1 - T_a/T_1)^2} - 0.5\right] \tag{5}$$

The DA consists in:

(1) Calculating, for each infill layout, the OOP strength by applying Eq. (1).
(2) Calculating, for each case study building and in each horizontal direction, the maximum demand acting on infills – which always occurs at the last floor – by using Eq. (4) and matching it to the capacity calculated using Eq. (1) in order to define the PSA_c.
(3) Calculating PGA_c from PSA_c using Eq. (5).

3. Reference Approach (RA)

For the application of RA, literature formulations for the assessment of the OOP capacity and demand are applied.

For what concerns the OOP capacity, i.e., the OOP strength model to be adopted, different proposals are provided in the literature. However, as shown in some studies (e.g., [32,33]), not all of them provide results in accordance with experimental data. A comprehensive study on this topic has been recently proposed by Di Domenico et al. [16].

In this study, for the prediction of the IP-undamaged infill OOP strength under seismic load, the mechanical model by Dawe and Seah is applied for thin infills (WL). In fact, based on experimental data, Di Domenico et al. [16] showed that Dawe and Seah [5]'s mechanical model, which allows the calculation of the entire OOP force-displacement response of the infill, is the most effective in predicting the OOP strength of thin URM infills. The OOP force displacement-curve for WL infills predicted by Dawe and Seah is reported in Fig. 1.

Experimental values of the OOP strength of IP-undamaged URM thick and robust infills (SL) are not provided in the literature. For this reason, it seems conservative to propose for this type of infills the application of EC6 formulation. The effectiveness of this formulation was not assessed on experimental data, as above explained, but it is certainly conservative, as it neglects the contribution to strength of horizontal arching action. In addition, it is derived based on an application of the lower bound theorem of limit analysis [16]. It should be noted that EC6 formulation is dedicated to infills under uniformly-distributed load. Within the application of the RA, this formulation is adapted to the seismic load shape as reported in Di Domenico et al. [16], i.e., by multiplying Eq. (1) times a coefficient equal to 0.85. Clearly, the conservativeness of EC6 formulation for thick and robust infills may yield to a conservative evaluation of the OOP seismic capacity of URM infills.

As above stated, the IP damage reduces the OOP strength of infills. R, the OOP strength degradation factor due to the IP damage, is calculated by applying the empirical relationship derived in Ricci et al. [30] and reported in Eq. (6). This formulation is based on experimental tests' results for URM infills in RC frames. The IP damage is represented

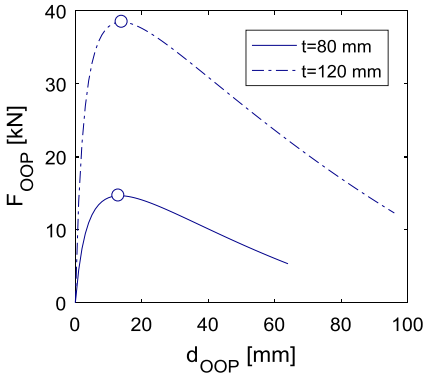

Fig. 1. OOP response curve of the 80 mm- and 120 mm-thick leafs predicted by applying Dawe and Seah's model.

by the maximum IP IDR demand, expressed in percentage, at given vertical slenderness (i.e., height-to-thickness) ratio, h/t.

$$R(IDR) = \frac{F_{Rd}(IDR|h/t)}{F_{Rd}(IDR = 0)} = \min(1; [1.21 - 0.05\min(20.4; h/t)](IDR)^{-0.89}) \quad (6)$$

The seismic demand on infills is obtained by multiplying the demand PSA times the infill mass participating to the first OOP vibration mode, equal, also in this case, to 66% of the infill total mass. Eq. (3) proposed by EC8 does not account for the effects of the nonlinear behaviour of the primary structure on floor acceleration demands while at LS the RC structure is supposed to have already experienced a significant nonlinearity [34]. Also for this reason, Eq. (3) may overestimate floor accelerations [35,36]. For this reason, within the RA, the OOP acceleration demand is calculated by using the floor spectra proposed for inelastic Multi-Degree of Freedom (MDOF) systems by Vukobratović and Fajfar [37]. Vukobratović and Fajfar [37] formulation of the PSA demand differs from EC8 proposal mainly for two aspects. First, it accounts for the effects of higher vibration modes, which are neglected in EC8 formulation: for this reason, for a given PGA – for example, 1 g – the acceleration demand may be not monotonically increasing along the building height as shown, for example, in Fig. 2a for a 6-storey case-study building. Second, it accounts for the inelastic structural behaviour associated with the first vibration mode by using the PSA reduction factor R_μ, which in this work is obtained from the SPO2IDA tool [38]. For this reason, for a given floor, the acceleration demand grows up with decreasing rate as PGA increases, as shown, for example, for the last storey of a 6-storey case-study building in Fig. 2b. The ductility of the non-structural element is considered by assigning to it an equivalent damping ratio, i.e., directly when calculating the PSA demand. For this reason, the force acting on infills is calculated without the application *a posteriori* of a behaviour factor. According to Vukobratović and Fajfar [37], such equivalent damping ratio is fixed to 10%, which is appropriate for non-structural elements with expected ductility demand equal to 1.5 (i.e., with ductility capacity at least equal to 1.5) and with 1% damping ratio, while it is conservative for non-structural elements at higher ductility demand and with higher damping ratio. It is worth to mention that previous studies [12] showed that, for both IP-undamaged and IP-damaged (up to moderate-high IDR levels) URM infills, the OOP ductility capacity is compatible with this value of minimum ductility capacity. Ongoing research is focused also on this issue, which is worth to be deepened.

For simplicity, the procedure is described with reference to a 4-storey building.

(1) For each infill layout, the OOP strength, F_{Rd}, is calculated by applying Dawe and Seah [5]'s model (for WL) or EC6 formulation (for SL).
(2) For each case-study infilled building, a static pushover (SPO) analysis is performed in the IP direction to obtain a base shear (V_b) vs roof displacement (Δ_{TOP}) curve. The loading path used to carry out SPO analyses is proportional to the force distribution along the frame height associated with the first vibration mode in the considered IP direction.
(3) The SPO V_b-Δ_{TOP} curve is then multi-linearized according to the piecewise procedure described for elastic-hardening-negative systems in De Luca et al. [39]. Note that the application of the above procedure results in an effective fundamental period assigned to each case-study building equal to its elastic fundamental vibration period.
(4) For each case-study building, the 50th percentile IDA curve is associated with each SPO curve by applying the SPO2IDA tool. This allows defining an elastic PSA vs Δ_{TOP} curve. The introduction of each elastic PSA in the EC8 Type I spectrum allows passing from elastic PSA to elastic PGA vs Δ curve. Using the SPO analysis results, with each Δ_{TOP} it is possible to associate the IDR for each storey and to define PGA vs IDR curves for each storey (Fig. 3).
(5) With each IDR demand, for each storey, it is possible to associate the degraded strength of the infills at that storey, by means of Eq. (6), and trace a PSA_c vs PGA_{IP} curve (Fig. 3).
(6) It is assumed that the PGA acting in the OOP direction is equal to the PGA acting in the IP direction. For each PGA_{OOP} value, the PSA demand, PSA_d, in the OOP direction is calculated by means of Vukobratović and Fajfar [37] floor spectrum and demand PSA vs PGA_{OOP} curves for each storey can be defined (Fig. 4a).
(7) The lower PGA at which the PSA_c vs PGA_{IP} and the demand PSA vs PGA_{OOP} curves intersect is the PGA_c accounting for the IP/OOP interaction associated with the considered building (Fig. 4b). For each case-study infilled building and for each infill layout the effective PGA_c is the minimum between the one calculated assuming X and Z as the IP direction, clearly. The IDR distribution associated with PGA_c is the collapse IDR distribution assessed by accounting for the IP/OOP interaction.

Due to the lack of exhaustive experimental data as well as of code provisions on this issue, the effects of OOP actions on the IP response of infills that were experimentally observed by some authors [23] are neglected. This approach, given the overestimation of the infilled structure stiffness, yields to a non-conservative underestimation of the infills IP displacement and, so, of their OOP capacity reduction due to interaction. Moreover, the infill OOP stiffness reduction due to IP actions observed by some authors (e.g., [29,30]) is neglected as well as

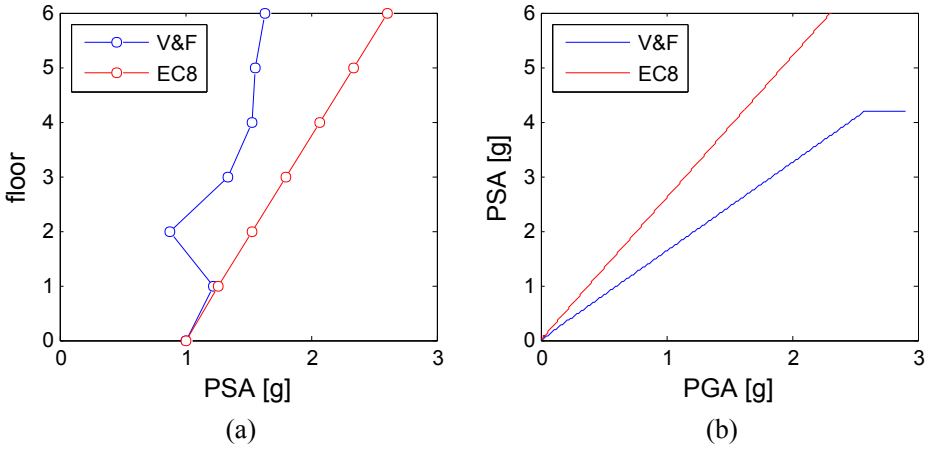

Fig. 2. Floor distribution of demand acceleration for given PGA equal to 1.00 g (a) and PSA evolution at increasing PGA for the last storey (b) of a 6-storey case-study building obtained by applying Vukobratovic and Fajfar's (V&F) and Eurocode 8's (EC8) floor spectrum.

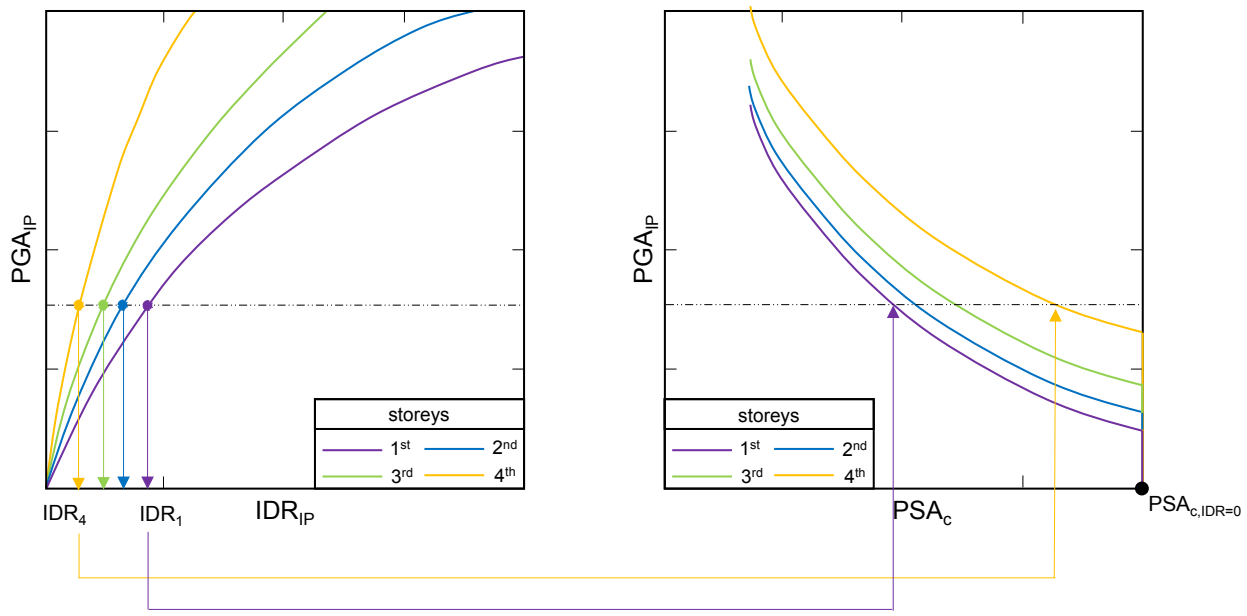

Fig. 3. Reference approach schematic representation: definition of IP displacement demand as a function of the IP PGA and definition of the degraded OOP strength of infills corresponding to that IP PGA.

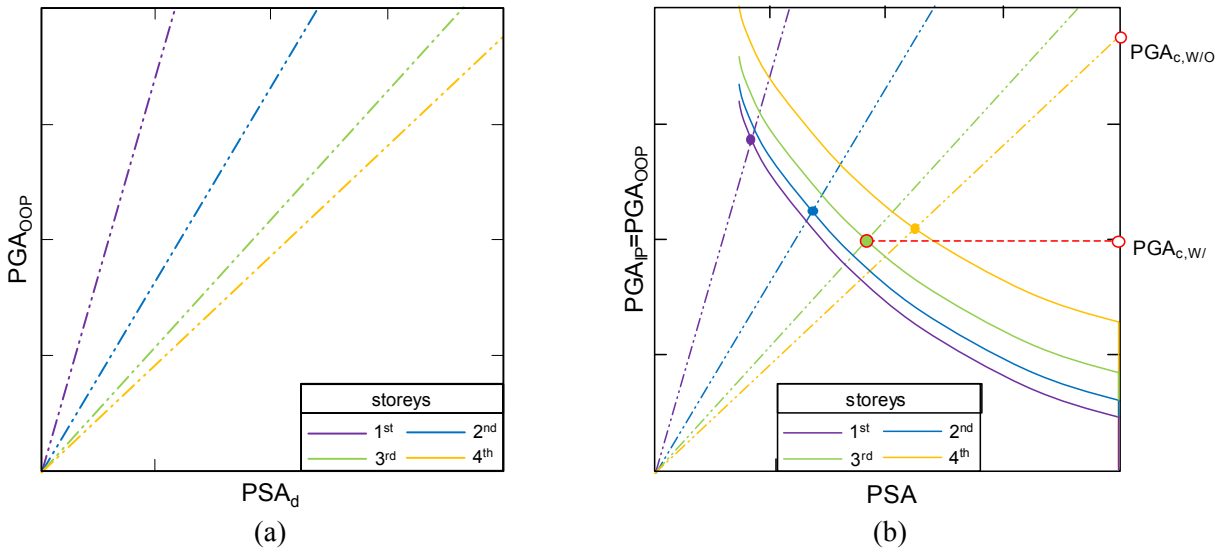

Fig. 4. Reference approach schematic representation: definition of OOP demand (a) and matching of OOP capacity and demand (b).

the consequent T_a elongation and the potential presence of openings.

4. Description of the case-study infilled frames

4.1. RC frames

Hereafter, the design in Ductility Class "High" (DCH) of 16 Category A (Domestic and Residential activities according to Eurocode 1 [40], section 6.3.1) RC buildings with rectangular plan is presented. The buildings consist of 5 and 3 bays in the X and Z direction, respectively. All bays spans are 4.5 m long while the inter-storey height is always equal to 3.0 m. Each building was designed for gravity and seismic loads by applying the Response Spectrum Analysis (RSA) method according to Eurocode 2 [41] and EC8. The 16 designed buildings are distinguished for the number of storeys (2, 4, 6, 8) and for the different values of the design PGA at LS (0.05 g, 0.15 g, 0.25 g, 0.35 g). The used materials are class C28/35 concrete and reinforcing steel with characteristic yielding stress equal to 450 N/mm^2. For the seismic design, the response spectrum provided for horizontal motion by EC8, section 3, was used. The vertical seismic component was neglected, as none of the conditions stated in EC8, section 4.3.3.5.2, was met. The buildings were designed on a stiff and horizontal type A soil, with soil factor S equal to 1. The importance factor γ_I was set to 1, the damping ratio was set to the 5%, the periods T_B, T_C and T_D were set to the ones suggested for the Type 1 elastic spectrum, which is recommended for high-seismicity zones. The elastic spectrum adopted for the design and assessment of the case-study buildings at Damage Limitation limit state (DL) was determined by multiplying by 0.40 the elastic spectrum adopted for the design and assessment at LS [2]. This value was determined as the ratio between the PGA at DL and the PGA at LS provided by the hazard curves defined by the Italian building code [42]. More specifically, according to the Italian hazard curves provided in the code, the ratio between the PGA on stiff and horizontal soil for T_R = 50 years (i.e., the return period of the design earthquake at DL for ordinary buildings) and the one for T_R = 475 years (i.e., the return period of the design earthquake at LS for ordinary buildings) is equal, on average, to 0.40, with a

standard deviation equal to 0.06 and a coefficient of variation equal to 15%.

Within the application of the RSA, for the force-based safety check of structural elements at LS, the elastic response spectra were reduced by dividing the spectral pseudo-accelerations by a behaviour factor q that was calculated according to Eq. (7), which is provided by in section 5.2.2.2 of EC8, for multi-storey and multi-bay RC framed systems regular in plan.

$$q = 4.5\frac{\alpha_u}{\alpha_1}k_w \quad (7)$$

In Eq. (7), α_u/α_1, the overstrength ratio, is assumed equal to 1.3 while k_w, the factor accounting for shear walls presence, is assumed equal to 1. With the application of a reduction factor equal to 0.8 due to the irregularity in elevation, the behaviour factor results equal to 4.68. The design of buildings as bare RC frames was carried out by applying the basic principles presented in section 4.2.1 of EC8. Among all, the diaphragmatic behavior of the storey levels was assured and introduced in the structural model, as well as a 50% reduction of the inertia of the structural members' cross sections was applied, according to EC8 (section 4.3.1(7)). The structural elements' dimensions were defined accounting for the lateral deformability limitation at DL, for the prevention of the bond failure of the anchorage of beams' reinforcement, according to section 5.6.2.2 of EC8, and to prevent significant P-δ effects. For seismic safety assessment, the seismic action was applied in two directions in the horizontal plan (X and Z) and its effect along X and Z were combined according to the 30% combination rule. To account for accidental torsional effects, the floor mass center was set in 4 different positions. Each one of the 4 application points was 5% of the structural plan dimensions in the X and Z direction apart from the floor geometric center (EC8, section 4.3.2). The plan and elevation regularity was verified according to the criteria listed in section 4.2.3 of EC8: all buildings were regular in plan and not regular in elevation due to a non-gradual stiffness reduction along their height. The negligibility of P-δ effects was verified according to EC8, section 4.4.2.2. For all buildings, lateral deformability verifications at DL limit state were performed. The displacements values were obtained by means of an elastic RSA. In all the considered cases, the maximum IDR was never larger than 2-3‰, so the verification was satisfied. The longitudinal and transverse reinforcement amount for beams and columns was determined according to force demands due to gravity and seismic loads assessed by using the RSA analysis and by applying capacity design rules.

In order to apply the RA described in section 2.2, The RC elements non-linearity was modelled by using a tri-linear moment-chord rotation backbone provided with the cracking point and perfectly plastic after yielding point. These points are determined using a section analysis and by applying the dispositions about yielding chord rotation given by the Annex A of EC8, part 3 [43].

4.2. Infill walls

As previously stated, two infill layouts are considered. The first one is constituted by a double-leaf (thickness: 80 + 120 mm) URM 'weak' infill wall (weak layout, WL), the second one is constituted by a one-leaf (thickness: 300 mm) URM 'strong' infill wall (strong layout, SL). The mechanical properties of these infills are those calculated for the masonry wallets tested by Calvi and Bolognini [24] for the WL and those by Guidi et al. [26] for the SL (Table 1). Note that the value of the masonry shear strength of Guidi et al. [26]'s specimen was not provided and so was set to 0.30 N/mm^2 according to Table 3.4 of EC6.

Each infill wall was introduced in the structural model by using a single equivalent strut whose nonlinear behaviour was modelled based on Panagiotakos and Fardis [44] proposal. According to this modelling approach, the slope of the softening branch of the force-displacement IP behavior relationship is a fraction p of the infill initial elastic stiffness, while the infill residual strength is herein set to zero. In Fardis [45] it is suggested to set p to a value between −1.5% and −5%. For the WL and SL leaves, a p value equal to −1.6% and −3.6%, respectively, was assumed. Such values yield to a prediction of the softening stiffness and ultimate IP displacement in good accordance with the experimental evidences shown by Calvi and Bolognini [24] (specimen 2) for p = −1.6% and by Guidi et al. [26] (specimen URM-U) for p = −3.6%. The IP behaviour characteristic points are reported in Table 2.

Table 1
Geometric and mechanical properties of all infill layouts.

Property	Symbol	Units			
Leaf thickness	t	[mm]	80	120	300
Height	h	[mm]	3000	3000	3000
Width	w	[mm]	4500	4500	4500
Slenderness ratio	h/t	[–]	37.5	25	10
Total mass	m_{tot}	[kg]	864	1296	3240
Shear modulus	G	[N/mm^2]	1039	1039	788
Shear strength	τ_{cr}	[N/mm^2]	0.15	0.15	0.30
Vertical direction					
Compressive strength	f_{mv}	[N/mm^2]	1.10	1.10	6.00
Elastic modulus	E_{mv}	[N/mm^2]	1873	1873	4312
Horizontal direction					
Compressive strength	f_{mh}	[N/mm^2]	1.11	1.11	1.19
Elastic modulus	E_{mh}	[N/mm^2]	991	991	1767

The dynamic properties of the case-study frames are reported in Tables 3 and 4. For instance, the design fundamental periods assessed for the structural models with halved inertia of primary elements, which are used when applying EC8 formulation for floor acceleration spectra, are reported for bare frames (Table 3) while the elastic fundamental periods, which are used when applying Vukobratović and Fajfar [37] formulation for floor acceleration spectra, are presented for the infilled frames (Table 4). As expected, at increasing number of storeys the vibration periods increase; on the contrary, at increasing design PGA at LS, the case-study buildings are characterized by elements with greater structural sections and, hence, by greater lateral stiffness. So, at increasing design PGA at LS, the vibration periods reduce.

In the following, each case-study building is identified by using an acronym, such as *XPY*, in which *X* is the number of storeys and *Y* the design PGA at LS expressed in g/100.

5. Application of DA and RA procedures

5.1. Designer Approach (DA) application and results

In this section, the results of the application of the procedure described in section 2.1 are presented and described. The OOP properties of the infills are reported in Table 5.

First, clearly, for given design PGA and number of storeys, a greater

Table 2
Infills' IP behaviour characteristic points.

Property	Symbol	Units			
Leaf thickness	t	[mm]	80	120	300
Cracking force	F_{crack}	[kN]	54.0	81.0	405
Initial stiffness	K_{crack}	[kN/mm]	125	187	355
Cracking displacement	d_{crack}	[mm]	0.43	0.43	1.14
Cracking IDR	IDR_{crack}	[%]	0.014	0.014	0.038
Maximum force	F_{max}	[kN]	70.0	105	526
Secant stiffness at max.	K_{max}	[kN/mm]	7.66	11.0	42.4
Displ. at maximum	d_{max}	[mm]	9.16	9.54	12.4
IDR at maximum	IDR_{max}	[%]	0.30	0.32	0.41
Collapse displacement	d_u	[mm]	44.3	44.7	53.7
Collapse IDR	IDR_u	[%]	1.48	1.49	1.79

Table 3
Design fundamental periods in the X and Z global directions of the case-study bare buildings.

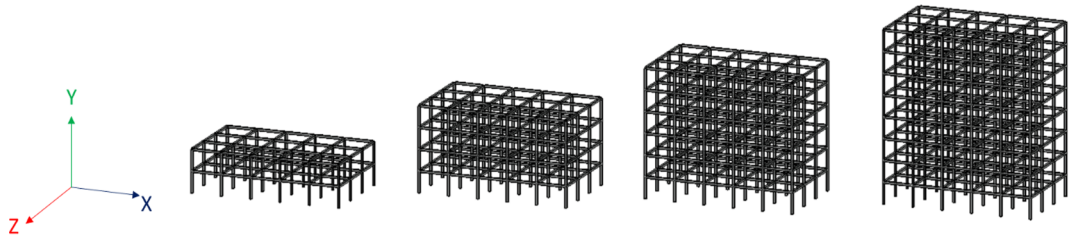

	Number of storeys of the infilled buildings							
	2		4		6		8	
design PGA at LS	$T_{1,Z}$ [s]	$T_{1,X}$ [s]	$T_{1,Z}$ [s]	$T_{1,X}$ [s]	$T_{1,Z}$ [s]	$T_{1,X}$ [s]	$T_{1,Z}$ [s]	$T_{1,X}$ [s]
0.05 g	0.418	0.406	0.578	0.554	0.775	0.743	1.070	1.023
0.15 g	0.418	0.406	0.538	0.520	0.741	0.712	1.022	0.977
0.25 g	0.418	0.406	0.476	0.459	0.693	0.665	0.961	0.919
0.35 g	0.345	0.336	0.403	0.389	0.566	0.542	0.762	0.728

Table 4
Elastic fundamental periods in the X and Z global directions of the case-study infilled buildings.

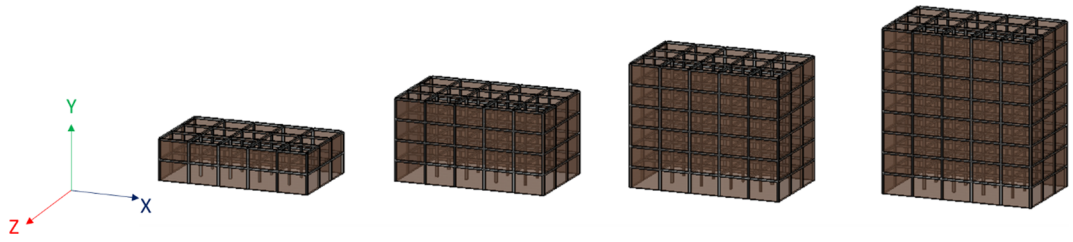

	Number of storeys of the infilled buildings							
	2		4		6		8	
design PGA at LS	$T_{1,Z}$ [s]	$T_{1,X}$ [s]	$T_{1,Z}$ [s]	$T_{1,X}$ [s]	$T_{1,Z}$ [s]	$T_{1,X}$ [s]	$T_{1,Z}$ [s]	$T_{1,X}$ [s]
WL								
0.05 g	0.107	0.085	0.222	0.181	0.298	0.242	0.414	0.329
0.15 g	0.107	0.085	0.219	0.177	0.293	0.240	0.408	0.326
0.25 g	0.107	0.085	0.210	0.178	0.277	0.231	0.386	0.315
0.35 g	0.104	0.083	0.209	0.176	0.277	0.231	0.384	0.318
SL								
0.05 g	0.103	0.085	0.215	0.173	0.293	0.233	0.407	0.317
0.15 g	0.103	0.085	0.211	0.172	0.289	0.231	0.401	0.315
0.25 g	0.103	0.085	0.206	0.169	0.275	0.224	0.383	0.309
0.35 g	0.102	0.084	0.205	0.168	0.272	0.226	0.381	0.306

Table 5
OOP infill properties for all layouts used for DA application.

Property	Symbol	Units			
Leaf thickness	t	[mm]	80	120	300
OOP strength	F_{Rd}	[kN]	10.6	23.8	810
PSA capacity	PSA_c	[g]	3.70	5.56	75.8*
OOP period	T_a	[s]	0.14	0.09	0.02

* Ratio of the OOP strength over the 66% of the infill weight, clearly without any physical acceptable meaning.

PGA_c is expected for SL than for WL, due to the different OOP strength associated with them.

If the IP/OOP interaction is neglected, as in this case, the first OOP infill collapse is always expected at the last storey. In fact, Eq. (5) proposed by EC8 predicts acceleration demands that monotonically grow up with the height of the barycenter of the considered non-structural element above the building base. This also means that, for the assessment of PGA_c with DA, the z/H ratio is fixed for all the case-study buildings with the same number of storeys and that the PGA_c associated with them varies only due to the variation of the infill layout and of the T_a/T_1 ratio. Eq. (5) returns acceleration demands that, for a given z/H, grows up with the T_a/T_1 ratio up to the resonance (i.e., for $T_a < T_1$). So, for a given infill layout and for a given number of storeys of the considered building, PGA_c decreases for increasing T_a/T_1 ratios, i.e., for increasing stiffness of the case-study bare frames, given that T_a is always lower than T_1. For this reason, the lower PGA_c is expected and registered for infills built along the Z direction, i.e., subjected to the OOP acceleration in the X direction, which is the buildings' stiffer direction. However, as shown in Fig. 5, the PGA_c in the two directions are very similar, with $PGA_{c,X}$ slightly lower than $PGA_{c,Z}$. So, in all cases, $PGA_{c,X}$ is the PGA_c of the case-study buildings.

Note that the capacity PGA values reported in Fig. 5b for SL infills are clearly without any physical meaning. Such a result in terms of PGA_c simply indicates that the OOP collapse of SL infills is practically impossible (according to DA). Moreover, a greater stiffness is expected for buildings designed for a greater PGA. For this reason, for a given

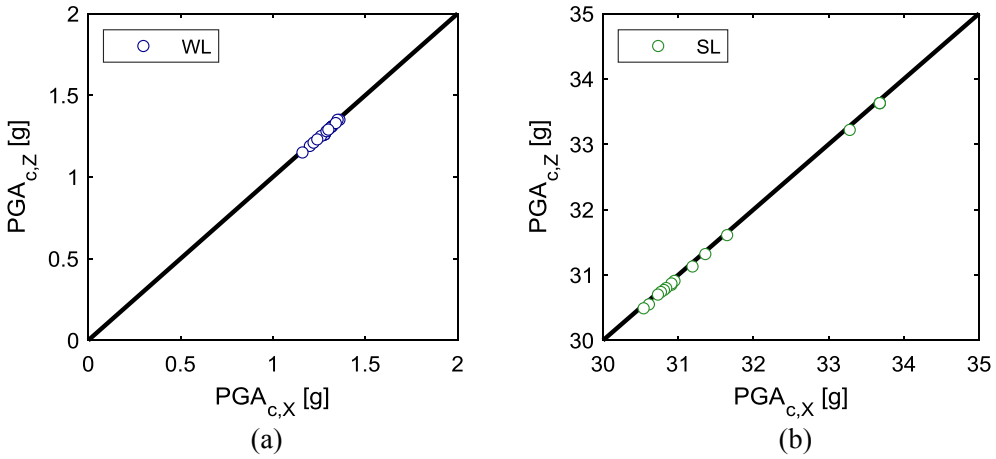

Fig. 5. Comparison of the OOP PGA_c in X and Z directions for WL infills (a) and SL infills (b) in all case-study buildings obtained by applying the DA.

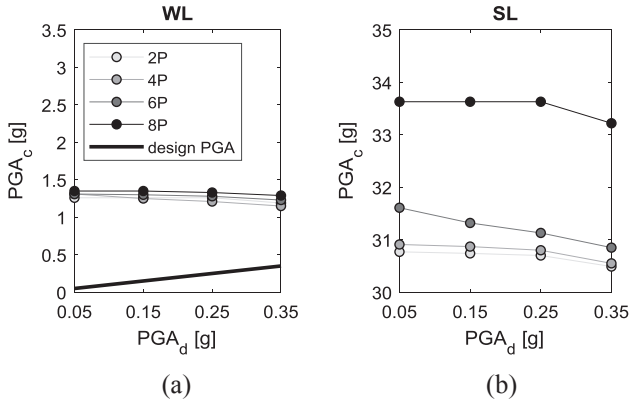

Fig. 6. Comparison of the OOP PGA_c for WL infills (a) and SL infills (b) in all case-study buildings obtained by applying the DA. Effect of the design PGA.

infill layout and for a given number of storeys, PGA_c is expected to decrease for increasing design PGA (Fig. 6).

It is observed, from Fig. 6, that using DA always returns PGAs associated with the first OOP collapse of infills greater than the design PGA at LS. In other words, the DA usually makes the practitioner sure that the safety check of infills with respect to the OOP collapse is satisfied for common infill layouts with a demand-to-capacity ratio at most equal to around 0.30.

Moreover, for a given infill layout, i.e., for a given T_a, a lower T_1 is expected for buildings with a lower number of storeys, so a lower PGA_c is expected for lower buildings (Fig. 7).

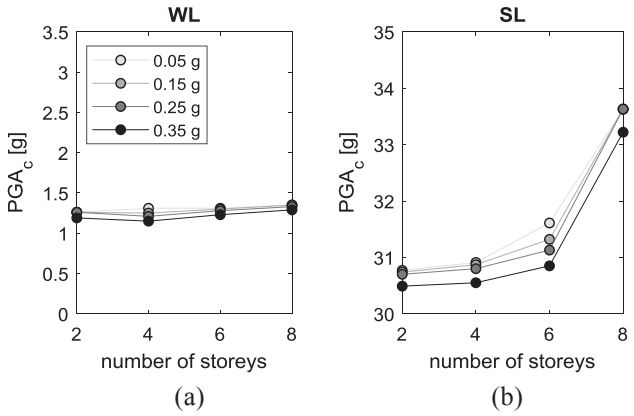

Fig. 7. Comparison of the OOP PGA_c for WL infills (a) and SL infills (b) in all case-study buildings obtained by applying the DA. Effect of the number of storeys.

However, these are not general rules, because some T_a/T_1-z/H combinations can result in lower PGA_c values assessed for taller buildings. For example, building 2P35 with WL infills has greater PGA_c than building 4P35 with the same infills. In the first case, $T_a/T_1 = 0.42$ and $z/H = 0.750$, while in the second case $T_a/T_1 = 0.36$ and $z/H = 0.875$. As shown in Fig. 8, for such T_a/T_1-z/H combinations, PGA_c is expected to be lower for 4P35 building.

6. Reference Approach (RA) application and results

In this section, the results of the application of the procedure reported in section 2.2. are presented and described. The OOP properties of the infills are reported in Table 6.

Note that the application of the RA yields to OOP strength values greater than those calculated by means of the EC6 formulation (in its original form) applied within the DA in the case of thin leaves. Mainly,

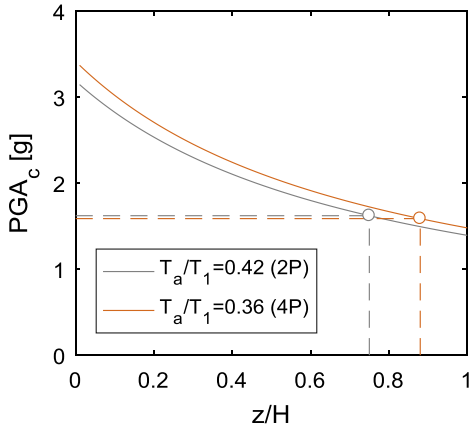

Fig. 8. PGA_c variation with z/H for fixed T_a/T_1 ratios.

Table 6
OOP infill properties for all layouts used for RA application.

Property	Symbol	Units			
Leaf thickness	t	[mm]	80	120	300
OOP strength	F_{Rd}	[kN]	14.7	38.5	688
PSA capacity	PSA_c	[g]	3.58	5.23	32.8*
OOP period	T_a	[s]	0.14	0.09	0.02

* Ratio of the OOP strength over the 66% of the infill weight, clearly without any physical acceptable meaning.

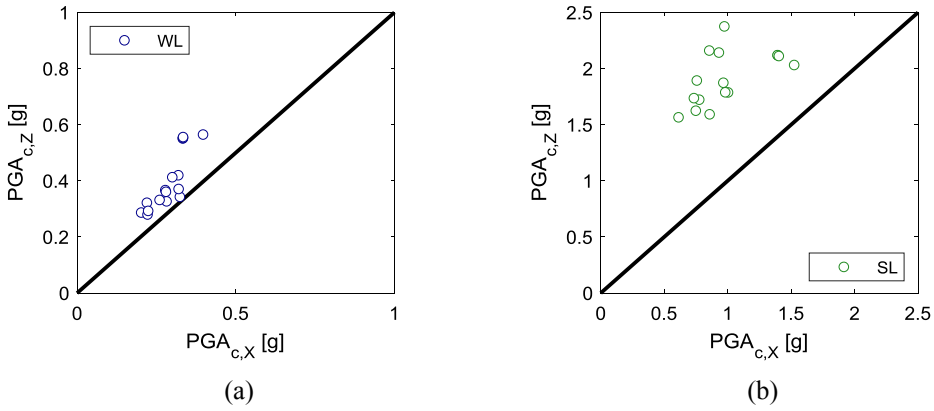

Fig. 9. Comparison of the OOP PGA_c in X and Z directions for WL infills (a) and SL infills (b) in all case-study buildings obtained by applying the RA.

this occurs since Dawe and Seah [5]'s model accounts for two-way arching, while EC6 formulation accounts only for vertical arching [16]. However, the strength obtained for the thick leaf is lower than that used for the application of the DA. This occurs because the strength model used for DA and RA is the same, but in the application of the RA the formulation by EC6 is modified to be adapted to the seismic loading condition [16]. In addition, note that being the 80 mm- and 120 mm-thick leaves' strength greater than that obtained by applying EC6 model, the lower PGA_c values obtained for them by applying the RA are only due to the different approach used in determining it, above all for the fact that in the RA the IP/OOP interaction is considered.

First, for a given design PGA and number of storeys, a greater PGA_c is expected for SL than for WL, due to the different OOP "undamaged" strength associated with them.

If the IP/OOP interaction is considered, the first OOP collapse is not expected at the last storey, given that the maximum strength degradation occurs at low-intermediate storeys, where the maximum IDR demand is expected. Moreover, for equal PGA applied in the X and Z direction, greater IDRs are expected in the less stiff direction, which is the Z direction for all the case-buildings. This means that the first OOP collapse is expected for infills built along the Z direction, i.e., for infills subjected to the OOP action in X direction. As shown in Fig. 9, for each case-study building $PGA_{c,X}$ is lower than $PGA_{c,Z}$ and, for this reason, it is assumed as PGA_c of the building.

Due to the IP/OOP interaction, the first OOP collapse is observed in the lower part of the building, generally below the building mid-height, along the building less stiff direction, as shown in Fig. 10. In Fig. 10 it is also observed that the storey associated with the first OOP collapse tends to pass, in the 8-storey buildings, from the third (WL) to the fifth (SL), most likely due to significant changes in the inelastic displacement shapes and collapse mechanism of such buildings at increasing strength and stiffness of the infills.

The parameters that define the OOP demand according to EC8, z/H and T_a/T_1, also enter Vukobratović and Fajfar [37]'s floor spectrum, even if in a more complex and elaborated form. So, for simplicity, let us explain some trends observed for PGA_c variation among the case-study buildings with direct reference to these parameters.

First, consider that, as shown in Fig. 10, the first OOP collapse storey, i.e., the z/H ratio, is fixed, *de facto*, for all the case-study buildings with the same number of storeys. Due to IP/OOP interaction, the PGA_c associated with them varies only due to the variation of the IDR demand distribution, which depends on the lateral deformability of the structure, and of the T_a/T_1 ratio. First, it is shown in Fig. 11 that for a given infill layout and design PGA, PGA_c decreases for increasing number of storeys, which is expected given the higher period of taller buildings.

For a given infill layout, the variability of the T_a/T_1 is extremely limited for different design PGAs, due to the prevalent effect of the infills' stiffness in T_1 definition with respect to the characteristics of the RC structure. For these reasons, for a given infill layout and for a given number of storeys, the PGA_c is almost independent on the design PGA, as shown in Fig. 12.

According to the RA results, as shown in Fig. 12, thin URM infills characterized by low OOP resistance (WL) in mid- and high-rise buildings (from 4 to 8 storey) deigned for mid- and high-seismicity zones (from 0.25 g) can be unsafe with respect to the OOP collapse. This means that, in these cases, the attainment of LS is avoided in terms of structural performance at the design PGA, at which widespread OOP collapses of infills are expected, instead. In addition, especially for WL, the PGA associated with the first OOP failure ($PGA_{c,OOP}$) can be lower than the PGA associated with the structural failure ($PGA_{c,STR}$) with respect to LS, i.e., the attainment for the first time in an RC element of the structure of a chord rotation demand equal to ¾ of the ultimate chord rotation of the element (which was calculated according to Annex A to EC8, part 3), as shown in Fig. 13. This means that the LS can be attained due to non-structural collapse prior than for structural collapse.

The OOP collapse due to IP/OOP interaction is expected for a maximum IDR demand in the Z direction equal to, on average, 0.44% for WL. For SL, the first OOP collapse due to IP/OOP interaction occurs for maximum IDRs ranging between 3% and 6%, which are always greater than IDR_u, i.e., the IDR at the IP collapse. This means that the IP collapse always foreruns the OOP collapse for this type of infills. This also means, in the Authors' opinion, that the OOP safety check for SL can be neglected, as the attainment of LS due to non-structural failure occurs for IP failure first.

Actually, for a given infill layout, 16 values of IDR corresponding to the first OOP collapse of infills were obtained, one for each case-study building. Based on these results, fragility curves relating the probability of OOP failure to the IP IDR for each infill layout were obtained and are reported in Fig. 14.

The reader is strongly recommended to consider such fragility curves only as a concise and immediate summary of the results obtained. Such curves are aimed at highlighting the role of IP damage in promoting the OOP collapse of infills, the importance of IP/OOP interaction phenomena, and the non-negligibility of such phenomena in assessing the safety with respect to seismic action of URM infills and of RC structures. In fact, in the Authors' opinion, it is not possible, nor correct, to define a "threshold IDR" at which the OOP collapse can be considered as expected, even in a simplified and code-based framework. As observed in this section, IP/OOP interaction is a complex phenomenon, whose effects are influenced by structural dynamic behaviour and by structural and non-structural nonlinearity. In order to correctly assess the seismic safety of URM infills, a detailed analysis, accounting for all these effects, is recommended.

As expected, a greater fragility with respect to infills' OOP collapse

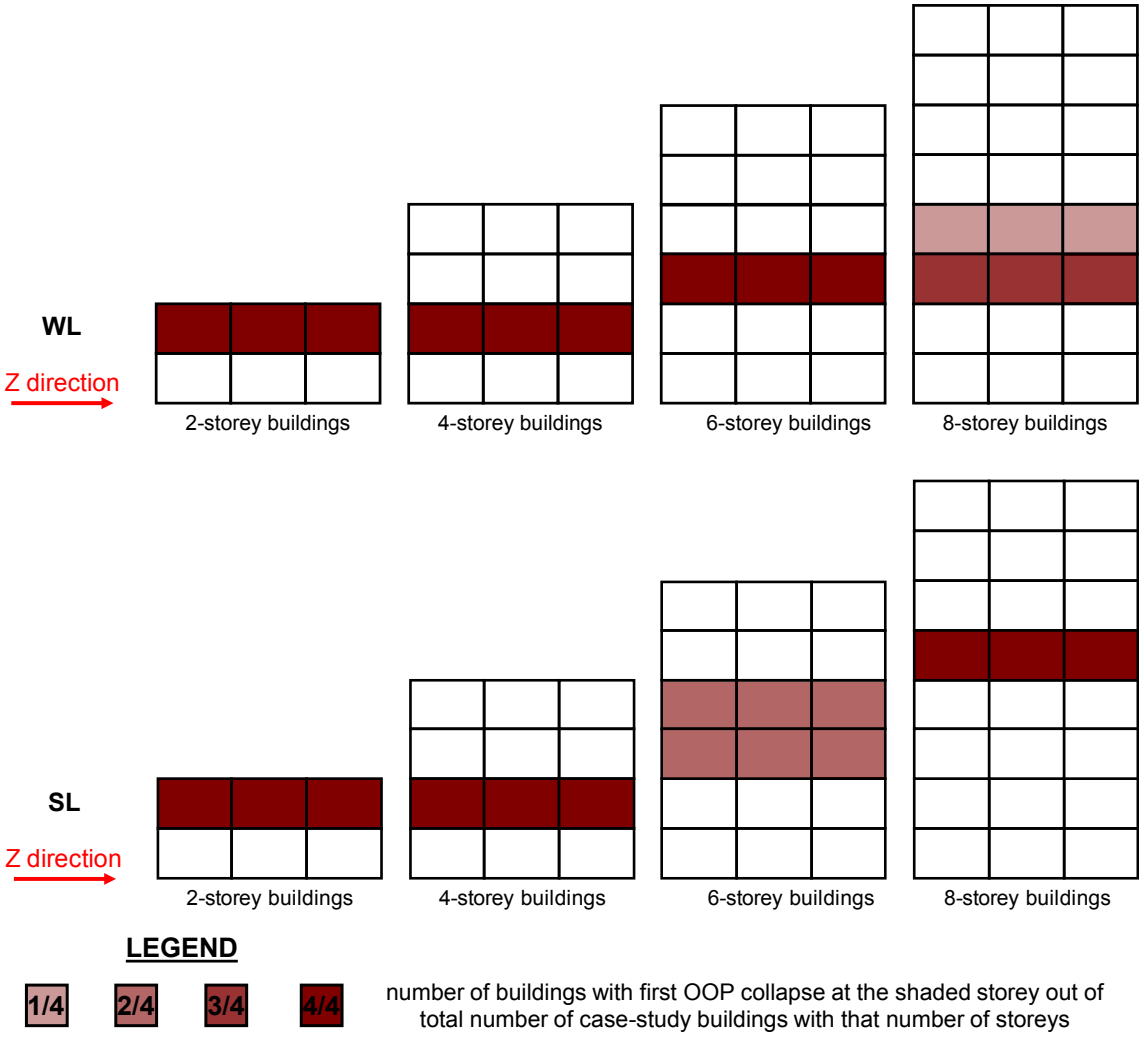

Fig. 10. Frequency distribution of floors at which the first OOP collapse occurs.

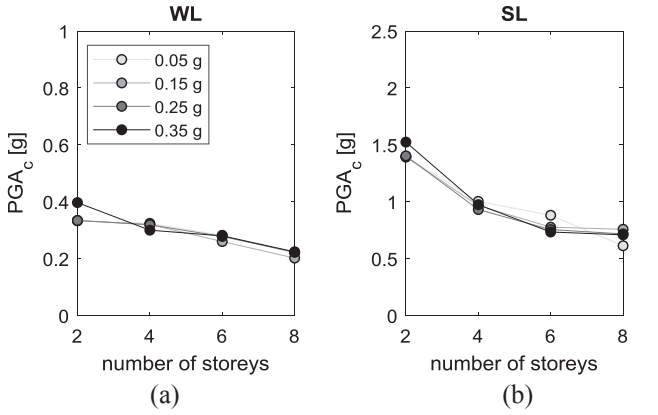

Fig. 11. Comparison of the OOP PGA_c for WL infills (a) and SL infills (b) in all case-study buildings obtained by applying the RA. Effect of the number of storeys.

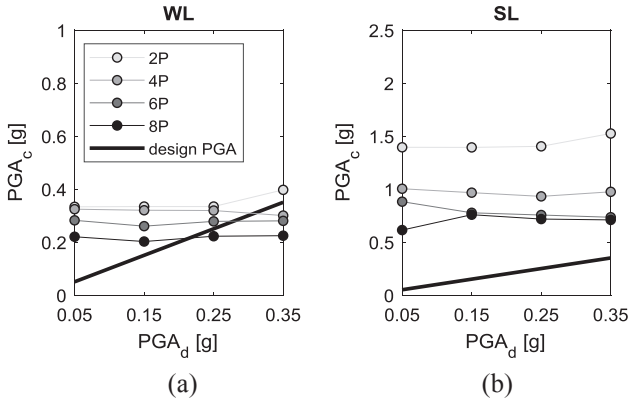

Fig. 12. Comparison of the OOP PGA_c for WL infills (a) and SL infills (b) in all case-study buildings obtained by applying the RA. Effect of the design PGA.

is observed for WL with respect to SL. Moreover, it is observed that the probability that the OOP collapse occurs for IDR lower than the IP collapse IDR, IDR_u, is around one for WL and around zero for SL. As already stated, this means that the attainment of LS due to non-structural failure occurs for OOP failure of thin/weak infills and for IP failure of thick/strong infills.

6.1. Comparison of DA and RA results

In Fig. 15, a comparison between the PGA_c predicted using the RA and the one obtained from the DA for each case-study building and for each infill layout is reported. As expected, PGA_c is highly overestimated using the DA. The PGA_c for WL obtained using the DA is, on average, 4.5 times the one obtained using the RA, while the PGA_c for SL obtained using the DA is, on average, 35 times the one obtained using the RA.

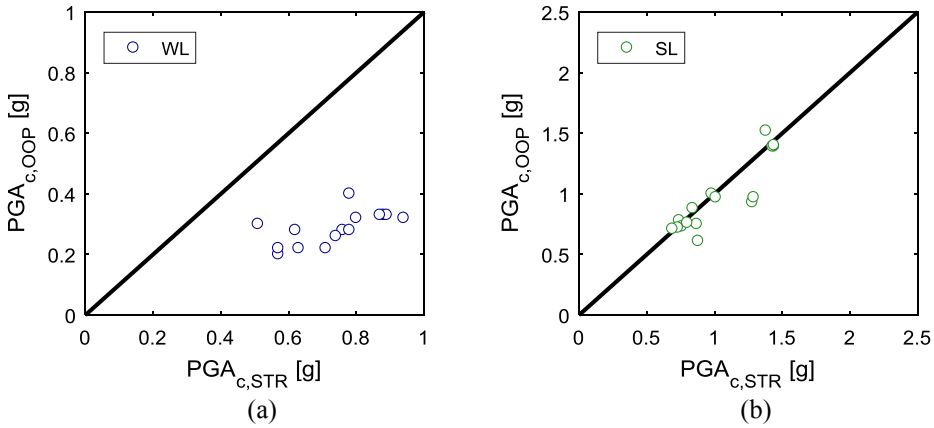

Fig. 13. Comparison of the PGA_c for WL infills (a) and SL infills (b) in all case-study buildings with respect to structural failure and non-structural OOP failure with respect to LS.

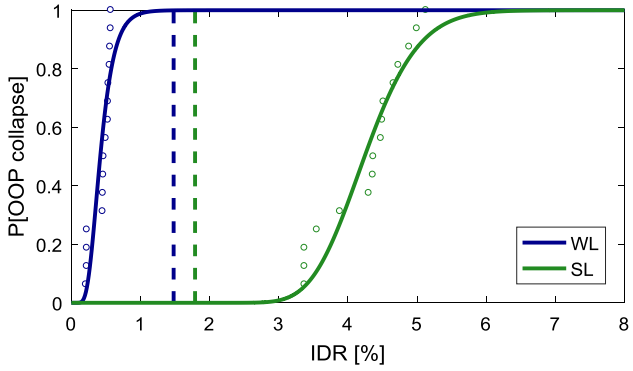

Fig. 14. Comparison of the fragility curves (continuous lines) in terms of IDR with respect to the attainment of LS for OOP failure of infills of all case-study buildings for different infill layouts. Dashed vertical lines represent the IDR corresponding to the IP collapse of the infill, according to Panagiotakos and Fardis's model.

For a given infill layout, 16 values of PGA corresponding to the first OOP collapse of infills were obtained by using both the DA and the RA, one for each case-study building. Based on these results, fragility curves relating the probability of OOP failure to the OOP PGA for each infill layout were obtained separately with reference to DA and RA results. These curves are reported in Fig. 16. The fragility curve for SL obtained by using the DA is not reported, given the high and physically unacceptable values of the collapse PGAs.

The median collapse PGA is equal to 0.29 g for WL, to 0.91 g for SL. As expected, a greater fragility with respect to infills' OOP collapse is

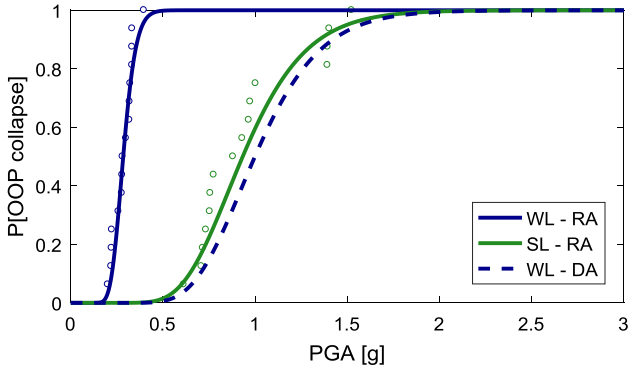

Fig. 16. Comparison of the fragility curves in terms of PGA, obtained by using the DA and RA, with respect to the attainment of LS for OOP failure of infills of all case-study buildings for different infill layouts.

observed if the RA is applied. A summary of the PGA_c values assessed using different approaches is reported in Table 7, at the end of next section.

7. OOP safety check of infills in a linear elastic framework

In this section, the PGA_c is assessed by applying an elastic RSA on the bare frame models of all case-study buildings. The OOP acceleration demand on infills is calculated by applying EC8 floor spectrum, while infills' OOP capacity is calculated using Dawe and Seah [5]'s model and the strength degradation curve proposed in Eq. (6), in which the IDR resulting from the RSA are introduced. This approach will be called

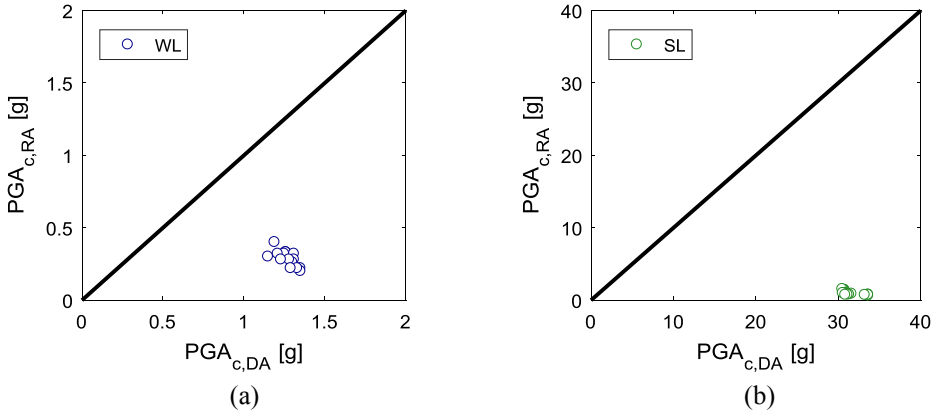

Fig. 15. Comparison of the OOP PGA_c for WL infills (a) and SL infills (b) in all case-study buildings obtained by applying the DA and RA.

Suggested Designer Approach (SDA). The main aim of this section is evaluating if the simplest and most common design procedure of RC buildings can be used to predict an accurate value of PGA_c if, at least, the IP/OOP interaction is considered. SL infills will be neglected, as it was demonstrated in the previous section that the OOP safety check for them can be omitted.

In this case, a fundamental role is played by the displacement distribution, and the consequent IDR distribution, along the building height resulting from the structural analysis. In fact, the OOP strength reduction factor is calculated based on such IDR distribution. First, let us investigate this issue: is the elastic distribution of IDRs along the building height appropriate to carry out infills' OOP safety check? Considering that the OOP safety check is not necessary for SL, as shown in the previous section, let us consider the elastic distribution of IDRs along the WL case-study buildings' height obtained by using a RSA with Response Spectrum anchored at the PGA_c evaluated, for each case-study building, using the RA. Moreover, in Fig. 17 the elastic IDR distribution is compared to the one obtained, at the same PGA value, using the RA.

As shown in Fig. 17, for mid- and high-rise buildings, the OOP strength reduction factor is underestimated if it is calculated based on the elastic distribution of IDRs obtained by applying the RSA on bare frame models. This unexpected result is strictly connected to the nonlinear response of the infilled frame assessed with the application of RA. In fact, except for the 2-storey case-study buildings, the top displacement demand at PGA_c is lower for the elastic bare frame model than for the infilled model, due to the non-negligible inelastic demand acting on it at PGA_c, as schematically shown in Fig. 18.

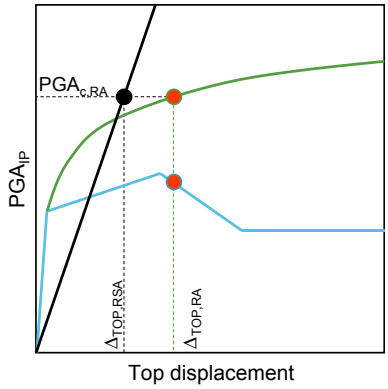

Fig. 18. Top displacement demand at PGA = $PGA_{c,RA}$ for the infilled and bare frame building. The static pushover of the infilled building is reported in blue, the SPO2IDA for the same building in green. The incremental response of the elastic bare frame is reported in black (schematic representation). (For interpretation of the references to colour in this figure legend, the reader is referred to the web version of this article.)

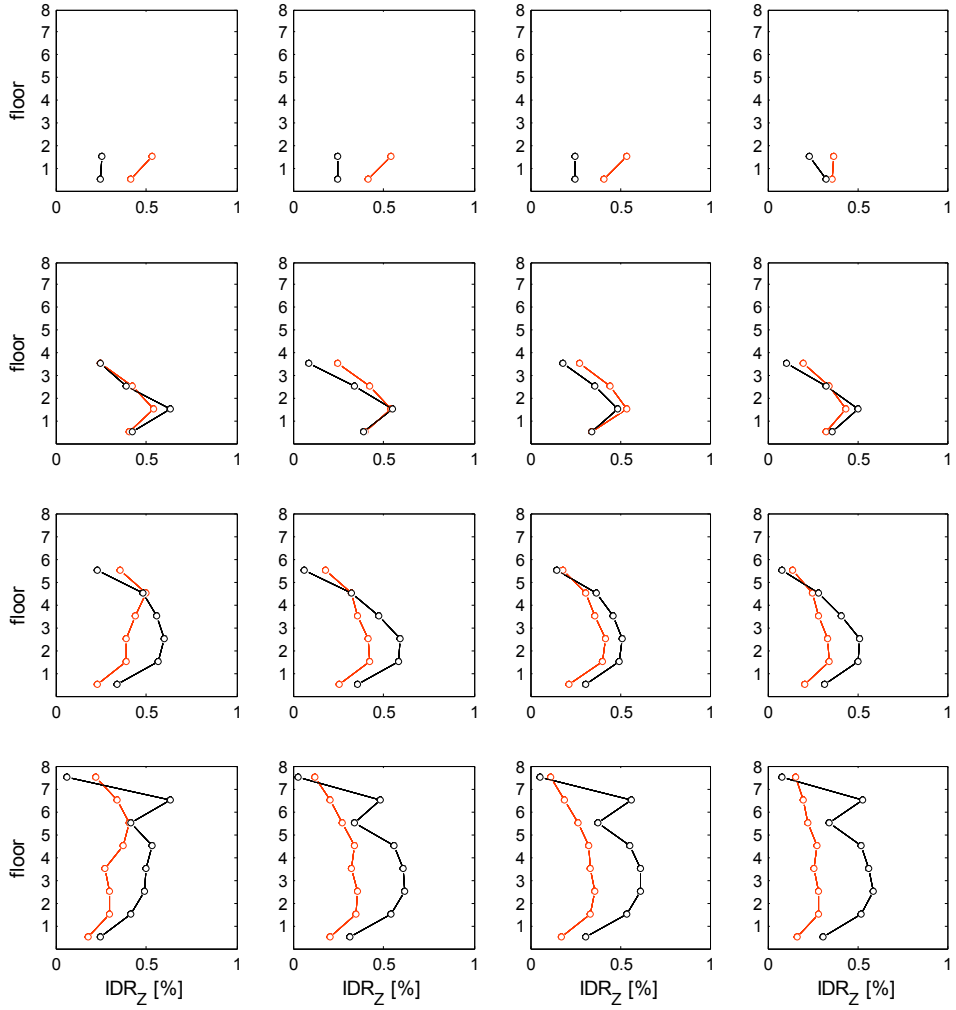

Fig. 17. IDR distribution in Z direction for all case-study buildings with WL infills obtained by means of RSA (red line) and nonlinear static analysis (black line) for PGA = $PGA_{c,RA}$. (For interpretation of the references to colour in this figure legend, the reader is referred to the web version of this article.)

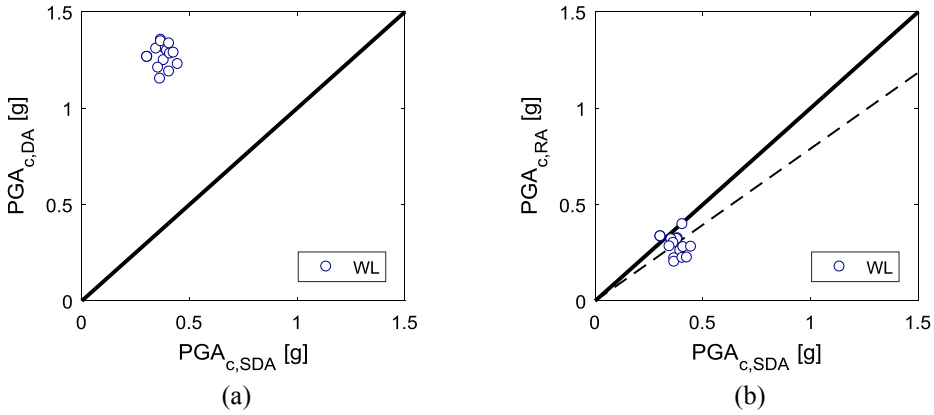

Fig. 19. Comparison of the OOP PGA_c in all case-study buildings obtained by applying the DA and SDA (a) and RA and SDA (b).

Table 7
PGA at first OOP infill collapse for all case-study buildings assessed by means of the Designer Approach (DA), Reference Approach (RA) and Suggested Designer Approach (SDA).

	First OOP collapse PGA [g]				
	WL			SL	
Case-study building	DA	RA	SDA	DA	RA
2P05	1.265	0.333	0.305	30.8	1.359
2P15	1.265	0.334	0.304	30.7	1.358
2P25	1.265	0.334	0.304	30.7	1.367
2P35	1.189	0.397	0.406	30.5	1.411
4P05	1.311	0.324	0.384	30.9	1.234
4P15	1.248	0.320	0.381	30.9	1.278
4P25	1.209	0.319	0.355	30.8	1.273
4P35	1.152	0.300	0.364	30.6	1.291
6P05	1.308	0.282	0.346	31.6	1.253
6P15	1.298	0.260	0.396	31.3	1.250
6P25	1.282	0.278	0.410	31.1	1.276
6P35	1.228	0.280	0.446	30.8	1.228
8P05	1.354	0.220	0.368	33.6	1.135
8P15	1.346	0.202	0.368	33.6	1.177
8P25	1.335	0.222	0.406	33.6	1.210
8P35	1.287	0.224	0.427	33.2	1.190

The nonlinear IDR distribution cannot be reproduced using elastic analyses on the bare frame models, which are destined to produce predictions of PGA_c, which are herein called $PGA_{c,SDA}$, greater than those obtained using the RA. In other words, a safety-check procedure not accounting for the inelastic response of the structure is not able to produce accurate values of PGA_c, for which the values obtained using the RA are assumed as benchmark in this work. The practitioner should be aware of this circumstance. Considering the observations discussed above, accounting for IP/OOP interaction, even if in a linear-elastic framework, is necessary to not overestimate PGA_c as shown in the comparison of DA and RA results, even if it is not sufficient to obtain an accurate prediction of PGA_c. In fact, such prediction cannot be other than un-conservative as long as the OOP safety check of infills is carried out in a linear elastic framework.

The values of PGA_c obtained by using the SDA for WL are compared to those obtained by means of DA and RA in Fig. 19a and b, respectively.

As already stated, accounting for IP/OOP interaction produces a reduction of PGA_c with respect to that predicted using the DA (Fig. 19a). However, PGA_c assessed using the SDA is generally greater than the benchmark one assessed using the RA (Fig. 19b): the ratio between the $PGA_{c,RA}$ and the $PGA_{c,SDA}$ for each case-study building ranges from 0.52 to 1.10 and is equal, on average, to 0.79.

In Table 7, the PGA_c assessed using the Designer Approach, the Reference Approach and the Suggested Designer Approach are reported for all case-study buildings. Remember that the capacity PGA values reported in Table 7 for SL infills, with reference to the DA, are clearly without any physical meaning. Such a result in terms of PGA_c simply indicates that the OOP collapse of SL infills is practically impossible (according to DA).

8. When is the OOP safety check of infills necessary?

As shown in section 4, SL infills, which are characterized by high compressive strength of masonry (f_m) and low slenderness ratio of the panel (i.e., the hight-to-thickness ratio, h/t), are expected to collapse for IP failure prior than for OOP failure. Let us call $PGA_{c,OOP}$ the PGA corresponding to the first OOP collapse and $PGA_{c,IP}$ the PGA corresponding to the first IP collapse, both calculated in a nonlinear static framework. The main aim of this section is defining, for each case-study building, a sort of "limit state" surface that can be used to know *a priori*, based only on the values of h/t and f_m, if each leaf of the infill walls of the building should be verified against the OOP collapse ($PGA_{c,OOP}/PGA_{c,IP} < 1$) or if the IP collapse foreruns the OOP collapse ($PGA_{c,OOP}/PGA_{c,IP} > 1$) and, so, the OOP safety check is not necessary, as the attainment of LS due to non-structural failure occurs for IP failure first. In this section, the application of the RA is carried out on all case-study buildings considering 42 different infill layouts generated by combining 7 different values of slenderness ratio (10, 12, 15, 20, 25, 30, 37.5) and 6 different values of masonry compressive strength in the vertical direction (1, 2, 3, 4, 5 and 6 N/mm^2). Among the 42 layout considered, 6 are associated with a single-leaf panel (h/t = 10) while the others are defined by a two-leaf panel constituted by a leaf with h/t equal to 12, 15, 20, 25, 30 or 37.5 plus a second leaf with slenderness equal to 37.5. For the double-leaf layouts, both leaves are provided with identical mechanical properties and the OOP strength is calculated by means of Dawe and Seah [5]'s model, while for single-leaf layouts the OOP strength is calculated by means of EC6 formulation adapted to the seismic loading condition.

Infill walls were IP-modelled by applying Panagiotakos and Fardis [44]'s model. Some assumptions have been made to define the IP and OOP behaviour of each infill layout.

(1) Based on Calvi and Bolognini [24] and Guidi et al. [26] experimental values of the compressive strength in the horizontal direction, which is equal to around 1 N/mm^2 for both Authors,

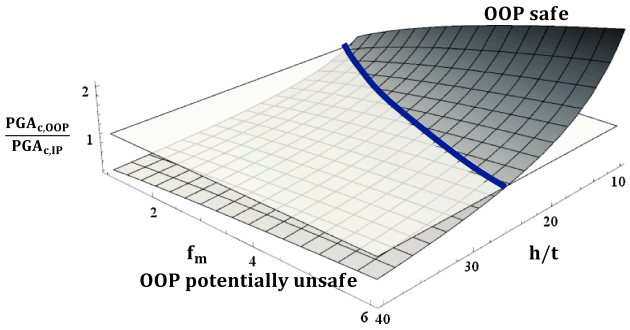

Fig. 20. Conceptual example of predicted $PGA_{c,OOP}/PGA_{c,IP}$ ratio surface (dark grey) with limit state curve (blue) separating the h/t-f_m couples for which the IP collapse foreruns the OOP collapse from those for which the OOP collapse foreruns the IP collapse. (For interpretation of the references to colour in this figure legend, the reader is referred to the web version of this article.)

independently on masonry compressive strength in the vertical direction, the same value was adopted for all infill layouts considered in this section;

(2) The elastic modulus of masonry in both horizontal and vertical direction has been calculated as 1000 times the masonry compressive strength in that direction, based on the relationship proposed in section 3.7.2 of EC6;
(3) The shear modulus of masonry has been assumed as equal to 0.4 times the elastic modulus calculated for the horizontal direction, in accordance with the recommendation reported in section 3.7.3 of EC6;
(4) Masonry tensile strength, τ_{cr}, has been determined as a function of masonry vertical compressive strength, f_m, by means of the linear interpolation of the τ_{cr}-f_m couples defined for Calvi and Bolognini [24] and for Guidi et al. [26],
(5) For the definition of the IP backbone, the softening stiffness ratio, p, has been determined as a function of the panel slenderness by means of a linear interpolation of the p-h/t couples defined for Calvi and Bolognini [24] and for Guidi et al. [26].

For each case-study building, the $PGA_{c,OOP}/PGA_{c,IP}$ ratio has been calculated for all 42 infill layouts. As shown in Fig. 20, the surface obtained by a linear least-square regression in the logarithmic space relating the considered h/t − f_m couples to the value of the $PGA_{c,OOP}/PGA_{c,IP}$ ratio can be represented in the h/t − f_m − $PGA_{c,OOP}/PGA_{c,IP}$ space. The intersection of this surface with the $PGA_{c,OOP}/PGA_{c,IP}$ = 1 plan is a curve whose projection on the h/t-f_m plan represents the "limit state" curve separating the h/t-f_m couples for which the IP collapse foreruns the OOP collapse (OOP safe infills) from those for which the OOP collapse foreruns the IP collapse (OOP potentially unsafe infills).

In Figs. 21–22, for each case-study building, the results of these calculations are reported in the h/t − f_m plan. Each h/t − f_m couple is represented by a point whose color indicates a specific condition:

- Blue points are associated with h/t-f_m couples for which $PGA_{c,OOP} < PGA_{c,IP}$;
- Green points represent h/t-f_m couples with $PGA_{c,OOP} > PGA_{c,IP}$ and $PGA_{c,OOP}$ greater than the design PGA at LS, i.e., h/t-f_m couples for which the OOP safety check is necessary but likely to be satisfied;
- Red points represent couples for which the OOP safety check is not satisfied, as $PGA_{c,OOP}$ is lower than the design PGA at LS.

For each case-study building, the "limit state" curve is represented in the h/t-f_m plan in blue. In addition, the curve corresponding to the intersection of the $PGA_{c,OOP}$/design PGA surface with the $PGA_{c,OOP}$/design PGA = 1 plan is reported in dark red. Such curve separates h/t-f_m couples for which the OOP safety check is satisfied from those for which the OOP safety check is not satisfied. For very low design PGA (i.e., for PGA = 0.05 g), the $PGA_{c,OOP}$/design PGA surface (which was obtained by a linear least-square regression in the logarithmic space) has no intersection with the $PGA_{c,OOP}$/design PGA = 1 plan. In these cases, no dark red curve is reported in Figs. 21–22.

It is shown in Figs. 21–22 that for slenderness ratios equal to or lower than 15 and masonry compressive strength in the vertical direction equal to at least 3 N/mm^2 the OOP safety check of URM infills can be neglected independently on the number of floors of the building and on its design PGA at LS, because the IP failure foreruns the OOP collapse. Note that, according to the formulation reported in section 3.6.1.2 of EC6, such a masonry compressive strength is attained for a brick compressive strength in the vertical direction and for a mortar compressive strength both equal to at least 5 N/mm^2. More in general, the minimum masonry compressive strength, $f_{m,min}$, that grants that the IP failure foreruns the OOP collapse can be expressed as a function of the h/t ratio, consistently with the blue curves reported in Figs. 21–22 and on the side of safety, according to Eq. (8), as also shown in Fig. 23.

$$f_{m,min}\,[N/mm^2] = 0.7(h/t - 10) + 1.5 \quad (8)$$

In addition, from Figs. 21–22, it is observed that, independently on the number of storeys of the considered building, for low PGA demand at LS only slender and weak URM infills are going to collapse. For buildings in high-seismicity zones, widespread OOP collapses are expected for infills with slenderness ratio equal to or greater than 20 and masonry compressive strength lower than 2 N/mm^2 and for infills with slenderness ratio equal to or greater than 30 independently on their masonry compressive strength.

9. Conclusions

In this work, 16 case-study buildings designed to Eurocodes, different for number of storeys (2, 4, 6 and 8) and design PGA (0.05 g, 0.15 g, 0.25 g and 0.35 g) are considered as uniformly infilled by two different infill layouts, a two-leaf "weak" infill layout (WL) and a one-leaf "strong" infill layout (SL). For these case-study buildings, the PGA at which the first OOP infill collapse occurs (PGA_c) has been evaluated by means of a "Designer Approach", which is based on code provisions and does not account for the IP/OOP interaction and for the structural non-linearity, and by means of a "Reference Approach", which accounts for the IP/OOP interaction and for the structural non-linearity in a nonlinear static framework. The following main conclusions can be drawn.

- Based on the application of the DA, the first OOP collapse is always expected at the building last storey. The PGA_c is always greater than the design PGA of the building at LS, i.e., all the case-study buildings are safe, according to current code provisions, against the OOP collapse of infills.
- Based on the application of the RA, the first OOP collapse is registered at the second storey for 2- and 4-storeys building while it is expected between the third and the fifth storey for 6- and 8-storeys buildings. By comparing the PGA_c to the design PGA at LS, URM infills characterized by low/intermediate OOP resistance (WL) in mid- and high-rise buildings (from 4 to 8 storey) designed for mid- and high-seismicity zones (PGA equal to 0.25 or 0.35 g) may be unsafe with respect to the occurrence of OOP collapses. This means that, in these cases, the attainment of LS is governed by the infill OOP collapse instead of the structural collapse, and it occurs for a PGA lower than the design PGA.

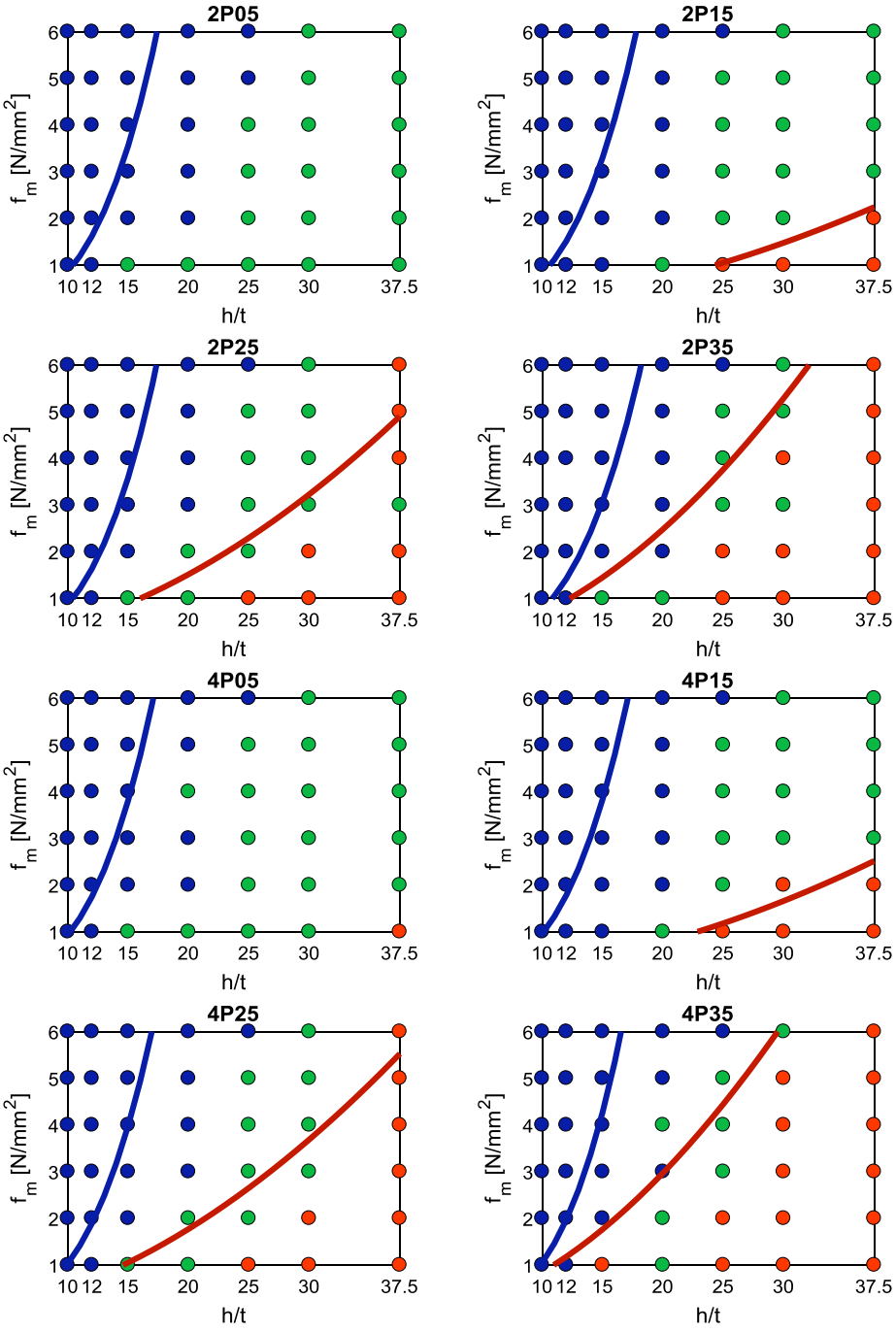

Fig. 21. OOP safety domains in terms of slenderness ratio and masonry compressive strength obtained for the 2- and 4-storey case-study buildings by applying the RA.

- Based on the RA results, fragility curves relating the probability of OOP collapse to both the PGA acting in the OOP direction and the maximum IDR attained in the IP direction assumed as demand parameters are shown. Median PGA_c calculated by applying the RA are equal to 0.29 g and 0.91 g for WL and SL, respectively. Such values are equal to 0.23 and 0.03 times the corresponding median PGA_c obtained by applying the DA (i.e., current code provisions may be highly not conservative when assessing the safety against OOP collapses of URM infills). Moreover, it is shown that for strong and robust infills the IP collapse foreruns the OOP collapse and the OOP safety check is not necessary, given that LS is attained, considering non-structural elements, for infills' IP failure first.
- Finally, for all case-study buildings, a wide range of 42 infill layouts, different for slenderness and masonry compressive strength, is considered and a "limit state" curve defining the h/t-f_m couples for which the IP collapse foreruns the OOP collapse is reported. Based

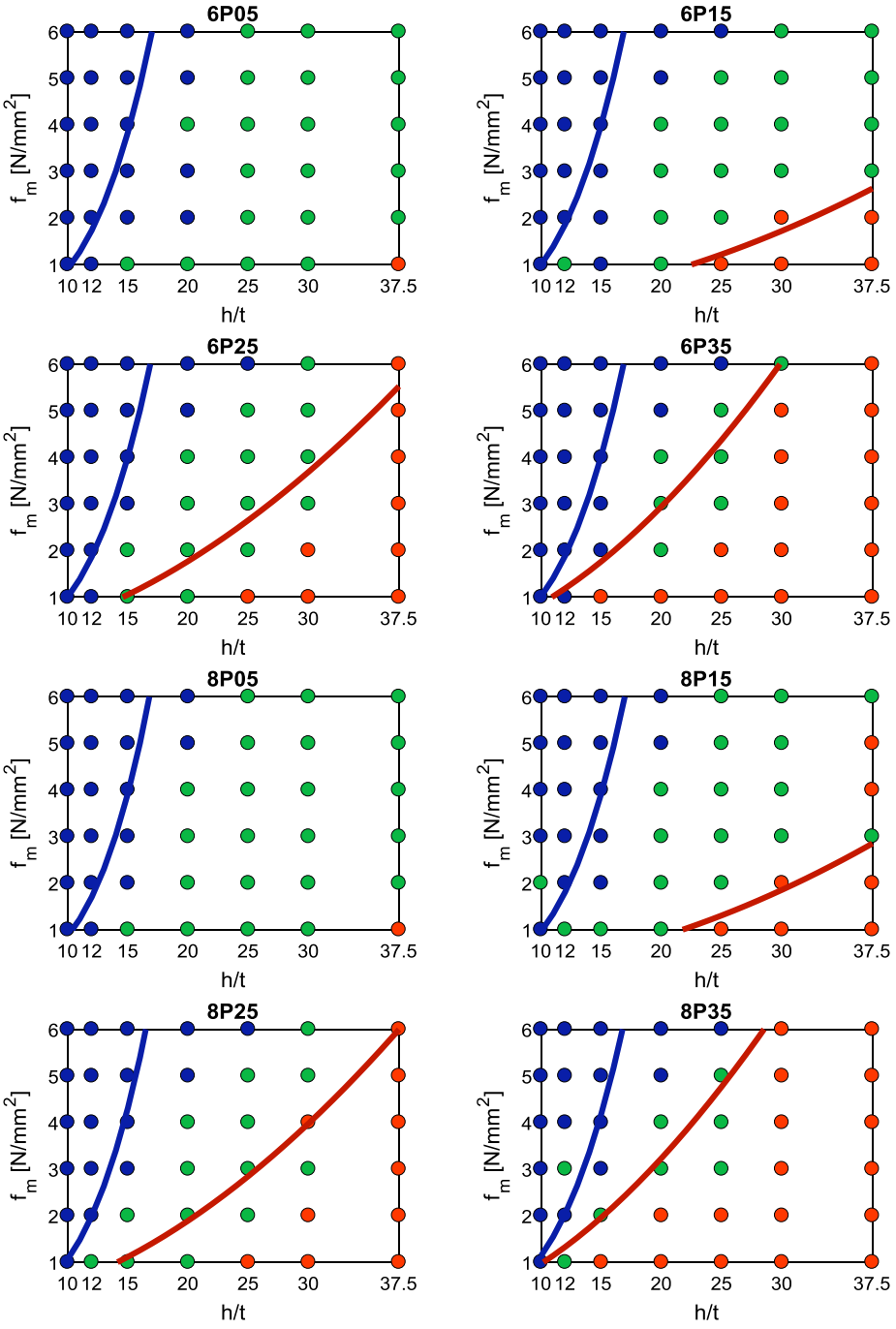

Fig. 22. OOP safety domains in terms of slenderness ratio and masonry compressive strength obtained for the 6- and 8-storey case-study buildings by applying the RA.

on these results, infills with slenderness equal to or lower than 15 and masonry compressive strength equal to or greater than 3 N/mm^2 are generally safe with respect to the OOP collapse, as it is forerun by IP failure, and the OOP safety check for them can be neglected.

In future works, the results reported in this paper will be compared with those obtained by means of non-linear time-history analyses on the case-study buildings herein presented. In this case, the OOP response of infills and the IP/OOP interaction effects will be explicitly modelled using the modelling strategy proposed by Ricci et al. [12]. The different structural performances assessed in a non-linear dynamic framework accounting for and neglecting the IP/OOP interaction phenomena will be compared. In addition, an OOP behaviour factor for URM infills will be defined, together with the effective stiffness that can be assigned to them in order to assess their OOP response in a linear elastic framework.

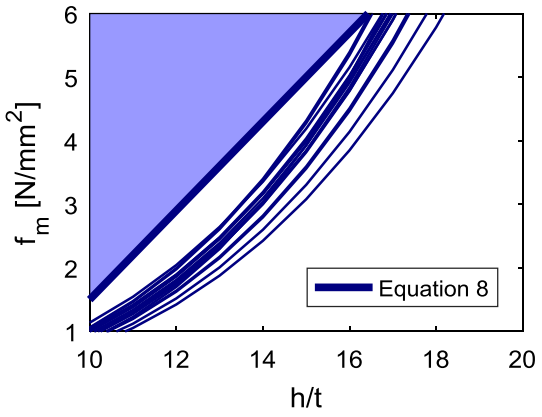

Fig. 23. Limit state curves for all case-study buildings and their linear safety-sided simplification. The shaded area covers all the OOP safe h/t-f_m couples.

Acknowledgements

This work was developed under the financial support of METROPOLIS (Metodologie e tecnologie integrate e sostenibili per l'adattamento e la sicurezza di sistemi urbani - PON Ricerca e Competitività 2007-2013) and ReLUIS-DPC 2014-2018 Linea Cemento Armato – WP6 Tamponature, funded by the Italian Department of Civil Protection (DPC). These supports are gratefully acknowledged.

The numerical analyses were carried out by using the computing and storage services provided by the ScOPE Datacenter of University of Naples Federico II. The support of the scientific and technical staff of the infrastructure is gratefully acknowledged.

Declaration of Competing Interest

The authors declare that they have no conflict of interest.

References

[1] Filiatrault A, Sullivan T. Performance-based seismic design of nonstructural building components: The next frontier of earthquake engineering. Earthq Eng Eng Vibrat 2001;13(1):17–46.
[2] Hak S, Morandi P, Magenes G, Sullivan TJ. Damage control for clay masonry infills in the design of RC frame structures. J Earthq Eng 2012;16(1):1–35.
[3] Sassun K, Sullivan TJ, Morandi P, Cardone D. Characterising the in-plane seismic performance of infill masonry. Bull New Zealand Soc Earthq Eng 2016;49(1):100–17.
[4] Taghavi S, Miranda E. Seismic performance and loss assessment of nonstructural building components. Proceedings of 7th National Conference on Earthquake Engineering. 2002.
[5] Dawe JL, Seah CK. Out-of-plane resistance of concrete masonry infilled panels. Can J Civ Eng 1989;16(6):854–64.
[6] Angel R, Abrams DP, Shapiro D, Uzarski J, Webster M. Behaviour of reinforced concrete frames with masonry infills. University of Illinois Engineering Experiment Station. College of Engineering. University of Illinois at Urbana-Champaign; 1994.
[7] Bashandy T, Rubiano NR, Klingner RE. Evaluation and analytical verification of infilled frame test data. Phil M. Ferguson Structural Engineering Laboratory, University of Texas at Austin; 1995.
[8] Flanagan RD, Bennett RM. Arching of masonry infilled frames: Comparison of analytical methods. Pract Periodical Struct Des Constr 1999;4(3):105–10.
[9] da Porto F, Barbiero E, Dalla Benetta C, Modena C. Sperimentazione sul comportamento fuori piano di tamponamenti in muratura di laterizio. Murature Oggi; 2007;94 [in Italian].
[10] Griffith MC, Vaculik J. Out-of-plane flexural strength of unreinforced clay brick masonry walls. TMS J 2007;25(1):53–68.
[11] Pasca M, Liberatore L. Predicting models for the evaluation of out-of-plane ultimate load carrying capacity of masonry infill walls. WIT Trans Built Environ 2015;152:83–94.
[12] Ricci P, Di Domenico M, Verderame GM. Empirical-based out-of-plane URM infill wall model accounting for the interaction with in-plane demand. Earthq Eng Struct Dyn 2018;47(3):802–27.
[13] Di Domenico M, Ricci P, Verderame GM. Experimental assessment of the influence of boundary conditions on the out-of-plane response of unreinforced masonry infill walls. J Earthq Eng. 2018 [in press] doi: https://doi.org/10.1080/13632469.2018.1453411.
[14] Di Trapani F, Cavaleri L, Shing PB. A macro-element model for in-plane and out-of-plane responses of masonry infills in frame structures. J Struct Eng 2018;144(2). https://doi.org/10.1061/(ASCE)ST.1943-541X.0001926.
[15] Di Domenico M, Ricci P, Verderame GM. Experimental assessment of the out-of-plane strength of URM infill walls with different slenderness and boundary conditions. Bull Earthq Eng 2019 [in press]. doi: https://doi.org/10.1007/s10518-019-00604-5.
[16] Di Domenico M, Ricci P, Verderame GM. Predicting the out-of-plane seismic strength of unreinforced masonry infills. J Earthq Eng 2019 [in press]. doi: https://doi.org/10.1080/13632469.2019.1604453.
[17] Eurocode 6. Design of Masonry Structures. Part 1-1: General Rules for Reinforced and Unreinforced Masonry Structures. Brussels; 2005. 123 p.
[18] FEMA 306. Evaluation of earthquake damaged concrete and masonry wall buildings, basic procedures manual. Washington, DC: Federal Emergency Management Agency; 1998.
[19] FEMA 356. Prestandard and commentary for the seismic rehabilitation of buildings. Washington, DC: Federal Emergency Management Agency; 2000.
[20] ASCE/SEI 41-13. Seismic rehabilitation of existing buildings. Reston, VA: American Society of Civil Engineers; 2013.
[21] ASCE/SEI 41-17. Seismic rehabilitation of existing buildings. Reston, VA: American Society of Civil Engineers; 2017.
[22] Eurocode 8. Design of structures for Earthquake Resistance. Part 1-1: General Rules, Seismic Actions and Rules for Buildings. Brussels; 2004. 229 p.
[23] Flanagan RD, Bennett RM. Bidirectional behaviour of structural clay tile infilled frames. J Struct Eng 1999;125(3):236–44.
[24] Calvi GM, Bolognini D. Seismic response of reinforced concrete frames infilled with weakly reinforced masonry panels. J Earthq Eng 2001;5(2):153–85.
[25] Kadysiewski S, Mosalam KM. Modelling of unreinforced masonry infill walls considering in-plane and out-of-plane interaction. Pacific Earthq Eng Res Center 2009.
[26] Guidi G, da Porto F, Dalla Benetta M, Verlato N, Modena C. Comportamento sperimentale nel piano e fuori piano di tamponamenti in muratura armata e rinforzata. Proceedings of the XV ANIDIS, L'Ingegneria Sismica in Italia, Padua, Italy; 2013, 30 [in Italian].
[27] Hak S, Morandi P, Magenes G. Out-of-plane experimental response of strong masonry infills. 2 nd European Conference on Earthquake Engineering and Seismology. 2014.
[28] Furtado A, Rodrigues H, Arêde A, Varum H. Experimental evaluation of out-of-plane capacity of masonry infill walls. Eng Struct 2016;111:48–63.
[29] Ricci P, Di Domenico M, Verderame GM. Experimental assessment of the in-plane/out-of-plane interaction in unreinforced masonry infill walls. Eng Struct 2018;2018(173):960–78.
[30] Ricci P, Di Domenico M, Verderame GM. Experimental investigation of the influence of slenderness ratio and of the in-plane/out-of-plane interaction on the out-of-plane strength of URM infill walls. Constr Build Mater 2018;2018(191):505–22.
[31] Timoshenko SP, Woinowsky Krieger S. Theory of plates and shells. New York: McGraw-Hill; 1959.
[32] Asteris PG, Cavaleri L, Di Trapani F, Tsaris AK. Numerical modelling of out-of-plane response of infilled frames: State of the art and future challenges for the equivalent strut macromodels. Eng Struct 2017;132:110–22.
[33] Pasca M, Liberatore L, Masiani R. Reliability of analytical models for the prediction of out-of-plane capacity of masonry infills. Struct Eng Mech 2017;64(6):765–81.
[34] Vukobratović V, Fajfar P. A method for the direct estimation of floor acceleration spectra for elastic and inelastic MDOF structures. Earthq Eng Struct Dyn 2016;45:2495–511. https://doi.org/10.1002/eqe.2779.
[35] Pinkawa M, Hoffmeister B, Feldmann M. A critical review of current approaches on the determination of seismic force demands on nonstructural components. In: Proceedings of the 9th International Conference on Structural Dynamics EURODYN2014. Porto, Portugal; 30 June – 2 July 2014.
[36] Petrone C, Magliulo G, Manfredi G. Seismic demand on light acceleration-sensitive nonstructural components in European reinforced concrete buildings. Earthq Eng Struct Dyn 2015;44:1203–17. https://doi.org/10.1002/eqe.2508.
[37] Vukobratović V, Fajfar P. Code-oriented floor acceleration spectra for building structures. Bull Earthq Eng 2017;15(7):3013–26.
[38] Vamvatsikos D, Cornell CA. Direct estimation of the seismic demand and capacity of oscillators with multi-linear static pushovers through IDA. Earthq Eng Struct Dyn 2006;35(9):1097–117.
[39] De Luca F, Vamvatsikos D, Iervolino I. Near-optimal piecewise linear fits of static pushover capacity curves for equivalent SDOF analysis. Earthq Eng Struct Dyn 2013;42(4):523–43.
[40] Eurocode 1. Actions on structures. Part 1-1: General actions – Densities, self-weight, imposed loads for buildings. Brussels; 2002. 225 p.
[41] Eurocode 2. Design of Concrete Structures. Part 1-1: General Rules and Rules for Buildings. Brussels; 2004. 225 p.
[42] NTC2008. Decreto ministeriale 14 gennaio 2008 - Norme Tecniche per le Costruzioni NTC2008. Supplemento ordinario n. 30 Gazzetta Ufficiale 4 febbraio; 2008, n 29 [in Italian].
[43] Eurocode 8. Design of structures for Earthquake Resistance. Part 3: Assessment and Retrofitting of Buildings. Brussels; 2005. 89 p.
[44] Panagiotakos TB, Fardis MN. Seismic response of infilled RC frames structures. In: 11th World Conference on Earthquake Engineering. June 23-28, 1996, Acapulco, México.
[45] Fardis MN (editor). Experimental and numerical investigations on the seismic response of RC infilled frames and recommendations for code provisions, ECOEST/PREC8 Report No.6, Laboratorio Nacional de Engenharia Civil Publications, Lisbon; 1996.